

AD-A098 106

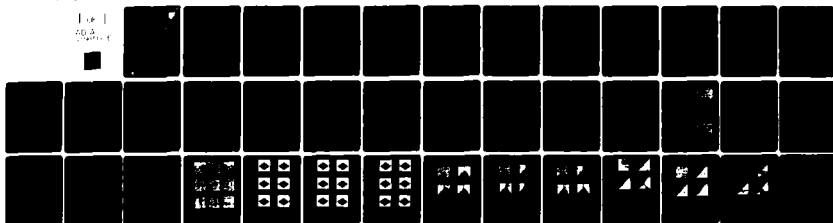
RENSSELAER POLYTECHNIC INST TROY NY DEPT OF ELECTRIC--ETC F/6 12/1  
FURTHER RESULTS ON TEXTURE DISCRIMINATION BASED UPON AN ASSUMED--ETC(U)  
MAR 81 A L VICKERS, J W MODESTINO F30602-78-C-0083

UNCLASSIFIED

RADC-TR-81-14

NL

Fig 1  
COA  
Figure 1



END

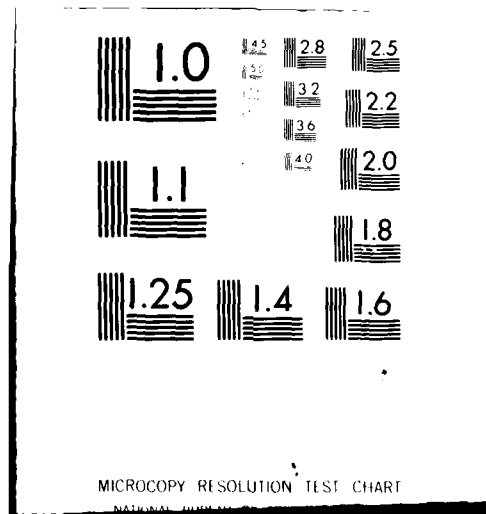
DATE

FILED

5-81

DTIC







AD A098106

**RADC-TR-81-14**  
**Final Technical Report**  
**March 1981**

**LEVEL II**



②

# **FURTHER RESULTS ON TEXTURE DISCRIMINATION BASED UPON AN ASSUMED STOCHASTIC TEXTURE MODEL**

**Rensselaer Polytechnic Institute**

**Acie L. Vickers**  
**James W. Modestino**

**DTIC**  
**ELECTE**  
**APR 23 1981**  
**S E D**

**APPROVED FOR PUBLIC RELEASE; DISTRIBUTION UNLIMITED**

**ROME AIR DEVELOPMENT CENTER**  
**Air Force Systems Command**  
**Griffiss Air Force Base, New York 13441**

**FILE COPY**

**81 4 23-043**

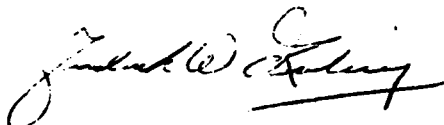


17

This report has been reviewed by the RADC Public Affairs Office (PA) and is releasable to the National Technical Information Service (NTIS). At NTIS it will be releasable to the general public, including foreign nations.

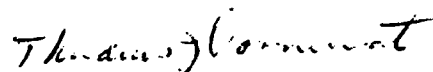
RADC-TR-81-14 has been reviewed and is approved for publication.

APPROVED:



FREDERICK W. RAHRIG  
Project Engineer

APPROVED:



THADEUS J. DOMURAT, Acting Chief  
Intelligence & Reconnaissance Division

FOR THE COMMANDER:



JOHN P. HUSS  
Acting Chief, Plans Office

If your address has changed or if you wish to be removed from the RADC mailing list, or if the addressee is no longer employed by your organization, please notify RADC (IRRE), Griffiss AFB NY 13441. This will assist us in maintaining a current mailing list.

Do not return this copy. Retain or destroy.



UNCLASSIFIED

SECURITY CLASSIFICATION OF THIS PAGE (When Data Entered)

19 REPORT DOCUMENTATION PAGE		READ INSTRUCTIONS BEFORE COMPLETING FORM	
1. REPORT NUMBER	2. GOVT ACCESSION NO.	3. RECIPIENT'S CATALOG NUMBER	
(12) RADC-TR-81-14	AD-A098106		
4. TITLE (and Subtitle)	5. TYPE OF REPORT & PERIOD COVERED	6. PERFORMING ORG. REPORT NUMBER	
(6) FURTHER RESULTS ON TEXTURE DISCRIMINATION BASED UPON AN ASSUMED STOCHASTIC TEXTURE MODEL	(9) Final Technical Report 4 Jan 81 - 31 Oct 81	N/A	
7. AUTHOR(s)	8. CONTRACT OR GRANT NUMBER(s)		
(13) Acie L./Vickers James W./Modestino	(15) F30602-78-C-0083		
9. PERFORMING ORGANIZATION NAME AND ADDRESS	10. PROGRAM ELEMENT, PROJECT, TASK AREA & WORK UNIT NUMBERS		
Rensselaer Polytechnic Institute Electrical & Systems Engineering Department Troy NY 12181	62702F 459418P2	(16)	(17) 18
11. CONTROLLING OFFICE NAME AND ADDRESS	12. REPORT DATE		
Rome Air Development Center (IRRE) Griffiss AFB NY 13441	(11) March 1981		
14. MONITORING AGENCY NAME & ADDRESS (if different from Controlling Office)	13. NUMBER OF PAGES		
Same	44		
	15. SECURITY CLASS. (of this report)		
(12) 4 p	UNCLASSIFIED		
	15a. DECLASSIFICATION/DOWNGRADING SCHEDULE		
	N/A		
16. DISTRIBUTION STATEMENT (of this Report)			
Approved for public release; distribution unlimited			
17. DISTRIBUTION STATEMENT (of the abstract entered in Block 20, if different from Report)			
Same			
18. SUPPLEMENTARY NOTES			
RADC Project Engineer: Frederick W. Rahrig (IRRE)			
19. KEY WORDS (Continue on reverse side if necessary and identify by block number)			
Texture Discrimination		Log-Likelihood Texture	
Stochastic Modeling		Discriminator	
Maximum Likelihood		2-D Digital Filtering	
Spatial Gray-Level Co-Occurrences			
20. ABSTRACT (Continue on reverse side if necessary and identify by block number)			
Further results of a new approach to texture discrimination are described. The approach is based upon an assumed stochastic model for texture in imagery and is an approximation to the statistically optimum maximum likelihood classifier. A method for estimating the structural parameters of the assumed stochastic texture model for each known texture class is described, and experimental results are provided which demonstrate the efficacy of this approach with simulated and real world texture data.			

DD FORM 1 JAN 73 1473 EDITION OF 1 NOV 55 IS OBSOLETE

UNCLASSIFIED

SECURITY CLASSIFICATION OF THIS PAGE (When Data Entered)

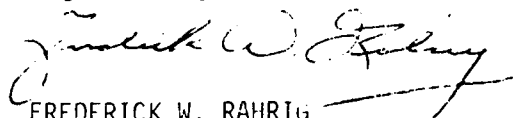
1/11/83

- 11



## EVALUATION

This report describes further results of an approach to texture discrimination based on spatial gray-level co-occurrences and maximum likelihood classification. Previous results demonstrated the capability of the log-likelihood texture discriminator to distinguish between random texture areas where other existing schemes could not. This procedure had the requirement that the model parameters for each of the texture classes be known a priori and were substituted into the discrimination process. A method has been developed for estimating the unknown parameters of the texture models through the incorporation of selecting representative training sets. This effort has created a technique that indicates an effective method for performing texture discrimination on real-world imagery. This work has provided a promising contribution to accomplishing the goals of technical planning objective R2B2A, Digital Image Exploitation.

  
FREDERICK W. RAHRIG  
Project Engineer

Accession For	
NTIS CNA&I	<input checked="" type="checkbox"/>
DTIC TAB	
Unannounced	
Justification	
By	
Distribution	
Availability Codes	
Availability	
Dist	Special
A	



## I. Introduction :

In [1], a new method of texture discrimination was proposed which made use of measurements of the spatial gray-level co-occurrence matrix described by Haralick and his co-workers [2]. The method was shown to be an approximation to the statistically optimum maximum likelihood classifier, and made use of explicit stochastic texture modeling assumptions. The construction and properties of several stochastic texture models were described and a 2-D digital filtering implementation of the resulting log-likelihood texture discriminant was provided. The efficacy of the approach was then demonstrated through experimental results obtained with simulated texture data.

Although the results presented in [1] were promising, the values of the model parameters for each of the texture classes known to be acting were assumed known a priori and were substituted into the log-likelihood discriminator directly. In practical applications involving real-world texture data, it is clear that the model parameters for each texture class known to be acting must be estimated by fitting an appropriate stochastic texture model to known samples from each texture class, and then substituting the estimated model parameters for each texture class into the log-likelihood discriminator.

In this paper a method will be presented for estimating the unknown structural parameters for the stochastic texture models described in [1]. This method for estimating the model parameters, like the log-likelihood discriminator, makes use of the spatial gray-level co-occurrence matrix and, following the logic used in developing the discriminator, will be shown to give approximate maximum likelihood estimates of the unknown model parameters.



After describing the overall discrimination system in Section II, a thorough description of the maximum likelihood parameter estimator is given in Section III. Results of the new parameter estimation technique are given in Section IV, while the efficacy of the log-likelihood discriminator which makes use of the parameter estimates is given in Section V. Section VI provides a summary and conclusion.

## II. Log-Likelihood Discriminator:

The block diagram which describes the log-likelihood texture discrimination system is presented in Fig. 1. All input image data which is to be processed by either the texture discriminator or parameter estimation stage is first passed through a pre-processing stage. The pre-processing stage serves two purposes. First, it provides a degree of normalization which eliminates undesirable effects such as differences in illumination, differences in digitization, etc. Secondly, it serves to re-quantize the data in a known fashion. It can be seen from [1] and the next section that both the discriminator and parameter estimator require knowledge of the scheme used in quantizing the data. This information may not be available in real-world applications. Even if the quantizing scheme were known, it may be necessary to re-quantize the data in order to make it suitable for processing by the discriminator or parameter estimator. An example is the number of gray levels. As seen in [1], the size of the spatial gray-level co-occurrence matrix is  $Q \times Q$ , where  $Q$  is the number of gray levels. Therefore, computational complexity of both the discriminator and estimator is proportional to  $Q^2$ , the square of the number of gray levels. For computational reasons, it is clear that  $Q$  should be chosen as small as possible. On the other hand, a value of  $Q$  chosen too



small will result in degraded performance. For the experiments described in this paper, a value of  $Q=64$  was found to provide satisfactory performance with reasonable computational cost. In any event, if the number of input image gray levels is larger than  $Q$ , some type of gray level conversion is necessary.

The type of pre-processing used in the experiments described here consisted of modifying the gray levels of the input data such that the resulting image possesses 64 gray levels and a Gaussian shaped histogram with a sample mean of 32 and a sample variance of 156.25. A typical input histogram of an image quantized to 256 gray-levels is illustrated in Fig. 2 together with the resulting output histogram after the image has been processed through the Gaussian histogram equalization process described above. The histogram modification technique used is described in Pratt [3], where the desired output probability density function (p.d.f.) is taken to be Gaussian with the mean and variance indicated above.

At first thought it may seem unreasonable to perform the histogram modification technique described above on the input data. By processing all the input images from all texture classes to have identical histograms, all first-order texture information, such as sample mean and sample variance, is lost. Some justification for performing this step can be found in the following argument. First-order statistics can be directly affected by changes of illumination or quantizing schemes, and thus the histogram equalization serves to remove these undesirable effects. More important, perhaps, is the fact that the proposed texture discriminator is designed to take advantage of second-order textural properties. If the texture classes to be processed possess markedly different distributions



properties, it is reasonable to assume that a simple discriminator based on first-order properties alone could be used instead of the proposed log-likelihood discriminator.

Once a decision has been made to perform histogram equalization on the input data, the choice of a Gaussian output histogram is easily explained. The stochastic texture models described in [1], which will be used as the underlying stochastic models for the various texture classes, all possess first-order Gaussian statistics. Thus, forcing the texture data to possess a Gaussian histogram will at least insure that there is not a first-order mismatch between the texture data and the model which is to be fitted by the parameter estimator.

The above pre-processing scheme is certainly not the only one which could be used. If the input data is properly quantized, then there may be no need to perform any processing at all. In fact, for the experiments involving synthetic textures, no pre-processing was done other than simple binary scaling of the input data from 256 to 64 gray levels.

After the original data is processed by the Gaussian equalization stage, it is divided into two groups. The first group consists of the training set, which consists of images containing only one texture whose class is known. This data is passed to the parameter estimator which looks individually at the texture data for each known class and attempts to fit the assumed underlying stochastic image model to each class. The unknown structural parameters are estimated for each class and used by the discriminator to form the log-likelihood functionals for each texture class as described in [1]. The second group of data consist of the unknown set; those images which are known to contain several textures



whose classes are unknown. This group of images is passed to the discriminator and processed as described in [1].

As can be seen, the discrimination system described here differs from that in [1] in that a training set must be available which contains known texture data from each of the possible classes, and a parameter estimator uses the training set to estimate unknown structural parameters for each texture class which were assumed known in the preliminary experiments conducted in [1]. Also, for real-world data, the pre-processing described above is used to normalize the data.

### III. Parameter Estimation Technique:

In this section a description of the techniques used to develop approximate maximum likelihood estimates of the unknown structural parameters is presented. It will be seen that development of the proposed estimator parallels almost exactly the development of the discriminator described in [1].

Recall from [1] that  $\{f_{i,j}\}_{i,j=1}^N$  is the input image and  $H_k$ ,  $k=0,1,\dots,K-1$  represent the  $K$  possible texture classes or hypotheses.

Also, recall that  $F_{i,j}$  represents the observations contained in a window of size  $(2M+1) \times (2M+1)$  centered about pixel position  $(i,j)$ . That is,

$$F_{i,j} = \{f_{k,l}, i-M \leq k \leq i+M, j-M \leq l \leq j+M\} \quad i,j=1,2,\dots,N, \quad (1)$$

where  $N$  is the total number of pixels along each side of the assumed square image array. From the data contained in this window the gray-level co-occurrence matrix was calculated for a fixed distance  $d$  for all rotation angles and was called  $P_{i,j}(d)$ . The log-likelihood classifier assigned the pixel  $(i,j)$  to the class  $Z(i,j)=k_0$  if



$$L_{k_0}\{P_{i,j}(d)\} = \max_{0 \leq k \leq K-1} L_k\{P_{i,j}(d)\}, \quad (2)$$

where

$$L_k\{P_{i,j}(d)\} \triangleq \ln \frac{p\{P_{i,j}(d)|H_k\}}{p_0\{P_{i,j}(d)\}} \quad k=0,1,\dots,K-1, \quad (3)$$

represents the class-conditional log-likelihood functional.

Now, instead of maximizing over the possible texture classes, it is proposed that the appropriate log-likelihood functionals be maximized over the range of unknown model values to determine approximate maximum likelihood estimates of unknown structural parameters. More precisely, let  $\{f_{i,j}\}_{i,j=1}^N$  now represent image data from the training set which is known to contain homogeneous texture data from only one class  $H_k$ . Assume that a suitable stochastic image model has been chosen and let  $\underline{a}$  represent the vector containing the model parameters which are unknown and have to be estimated from the gray-level co-occurrence matrix calculated from the data. Since the entire image is known to contain only one texture, the co-occurrence matrix can be calculated over the entire image and denoted  $P(d)$ . Also, let  $A$  represent the set of possible values which the unknown parameter vector  $\underline{a}$  may attain. The log-likelihood functional conditioned on  $H_k$  and parameter vector  $\underline{a}$  is then

$$L_k\{P(d);\underline{a}\} \triangleq \ln \frac{p\{P(d)|H_k, \underline{a}\}}{p_0\{P(d)\}}. \quad (4)$$

The approximate maximum likelihood estimate of the unknown parameter vector is the value which maximizes the log-likelihood functional of (4). That is, the maximum-likelihood estimator  $\hat{\underline{a}}_{ML}$  satisfies

$$L_k\{P(d);\hat{\underline{a}}_{ML}\} = \max_{\underline{a} \in A} L_k\{P(d);\underline{a}\}. \quad (5)$$



By comparing Eqs. (4) and (5) with Eqs. (1), (2), and (3), it can be seen that the proposed parameter estimation scheme follows the same logic and uses many of the elements of the previously proposed discrimination scheme. It is now necessary to specify a practical way of solving equation (5). The most common method is to take first derivatives and set the resulting equation to zero. That is, solve

$$\left. \frac{\partial L_k \{P(d); \underline{a}\}}{\partial \underline{a}} \right|_{\underline{a} = \hat{\underline{a}}_{ML}} = 0 \quad (6)$$

However, for the stochastic models which are of interest no closed form solution to (6) has yet been found. Therefore, it has been necessary to resort to a more direct but somewhat computational solution to equation (5). This involves performing a computer search over the permissible parameter space  $A$  and taking the value  $\hat{\underline{a}}_{ML}$  which maximizes (5). Since for a continuous parameter space, the range of possible values is uncountable, it is necessary to lay a discrete grid of points over the parameter space and evaluate the log-likelihood functional only at those points. Clearly, there is a tradeoff involved in specifying this grid. If the grid points are spaced too far apart, the calculated maximum may be far from the true maximum, resulting in poor parameter estimates. On the other hand, spacing the grid points too close together will result in an unnecessary computational burden.

It should be noted that more sophisticated search techniques than the one described above could be used to reduce the computational burden, but were not used due to their increased programming complexity.



At this point it is necessary to specify the underlying stochastic model to be used in the experiments described in the following experiments. The model chosen is the rectangular partition process described in [1]. From [1], it can be seen that

$$L_k\{P(d);\underline{a}\} = \sum_{m=0}^{Q-1} \sum_{n=0}^{Q-1} p(m,n;d) \lambda_k(m,n;d,\underline{a}) \quad , \quad (7)$$

where

$$\lambda_k(m,n;d,\underline{a}) = \ln Q_{m,n}(d;H_k,\underline{a}) \quad . \quad (8)$$

Recall that  $Q_{m,n}(d;H_k,\underline{a})$  is the probability of observing gray-levels  $m$  and  $n$  at a particular pair of points separated by a distance  $d$  conditioned on texture class  $H_k$  and parameter vector  $\underline{a}$ . Also, recall from [1] that

$$Q_{m,n}(d;H_k,\underline{a}) = \int_{E_m}^{E_{m+1}} \int_{E_n}^{E_{n+1}} p_k\{f_1, f_2; \underline{a}, d\Delta L\} \quad , \quad (9)$$

where  $E_l$ ,  $l=0,1,\dots,Q-1$  represent the quantization levels and  $\Delta L$  the spatial sampling interval.

For the rectangular partition process, the second-order p.d.f.  $p_k\{f_1, f_2; \underline{a}, d\Delta L\}$  in (9) can be evaluated<sup>†</sup> from corresponding results in [1].

$$p\{f_1, f_2; \underline{x}, \underline{x}+\underline{u}\} = \sum_{l=0}^{\infty} h_l(f_1, f_2) p_l(|\underline{u}|) \quad , \quad (10)$$

where

$$\begin{aligned} h_l(f_1, f_2) &= \frac{1}{2\pi\sigma^2\sqrt{1-\rho^{2l}}} \exp \left\{ -\frac{f_1^2 - 2\rho^l f_1 f_2 + f_2^2}{2\sigma^2(1-\rho^{2l})} \right\}; \quad l > 0 \\ &= \frac{1}{\sqrt{2\pi}\sigma} \exp \left\{ -\frac{f_1^2}{2\sigma^2} \right\} \delta(f_1 - f_2); \quad l = 0 \quad , \end{aligned} \quad (11)$$

<sup>†</sup> For notational convenience we have suppressed the conditioning on  $H_k$  and  $\underline{a}$  in (10) although this conditioning is clearly implicit.



and

$$p_l(||\underline{u}||) = \frac{4[\sqrt{2} \lambda ||\underline{u}||]}{\pi l!} \int_0^{\pi/2} \cos^l \theta \exp\{-\sqrt{2} \lambda ||\underline{u}|| \cos \theta\} d\theta \quad l=0,1,\dots \quad (12)$$

It can be seen that the rectangular process is completely defined in terms of the parameters  $\rho$ ,  $\lambda$ , and  $\sigma^2$ , representing the correlation coefficient, edge density, and variance of the random field, respectively. Due to the pre-processing stage, the variance  $\sigma^2$  will be known, and thus the unknown parameter vector  $\underline{a}$  consists of the parameters  $\lambda$  and  $\rho$ . That is  $\underline{a}^T = (\rho, \lambda)$ . Thus the search must be performed over a two dimensional grid of points. In the most general case,  $\rho$  and  $\lambda$  must obey  $-1 < \rho < 1$  and  $\lambda > 0$ . In practice, a priori knowledge of the textures of interest can be used to limit the search area to a much more manageable region.

#### IV. Parameter Estimation Results :

In order to establish the efficacy of the proposed parameter estimation technique, a two-dimensional search was first applied to synthetically generated realizations of the rectangular process to develop estimates of the parameters  $\rho$  and  $\lambda$ . The realizations used are shown in Fig. 3. Each of the images possesses 256 pixels to a side, has a mean and variance of 32 and 156.25, respectively, and is quantized to 64 gray levels. The grid which was used to generate the estimates covered a range of  $\rho$  from -0.1 to 0.8 and a range of  $\lambda$  from 0.1 to 0.4. The spacing between  $\rho$  values was 0.1 and the spacing between  $\lambda$  values



was 0.025. The grid region was chosen to encompass the actual parameter values for all the realizations so that the maximum values would be expected to fall within the search regions and not on a boundary. A comparison of the actual and estimated parameter values for each realization for various distances is presented in Table 1. It can be seen that the parameter estimates are quite good in all cases. Due to the grid spacings, it is difficult to determine which values of  $d$  provides the best result. The question of which value of  $d$  is best in general application of the parameter estimator and discriminator will be presented in Section VI.

It is of some interest to see how the value of the log-likelihood functional of (7) varies over the search grid. Three-dimensional plots of the resulting likelihood surfaces for the cases considered are illustrated in Fig.'s 4-12. The labeled axes represent the values of  $\rho$  and  $\lambda$  over which the search was performed while the remaining axis represents the value of the log-likelihood functional for the corresponding values of  $\rho$  and  $\lambda$ . It can be seen that the surfaces are generally quite smooth with no sharp peaks at the maximum.

After demonstrating that the estimator works for the synthetic image, it now is of interest to apply the parameter estimator to real-world imagery as a first step in a total texture discrimination approach. The test images used consist of selected samples of Brodatz textures [4]. Typical samples of grass, raffia, and herringbone are illustrated in Fig. 13. These images consist of  $256 \times 256$  pixels and have been processed by the Gaussian equalization stage described in Section II to possess 64 gray-levels, a mean of 32, and a variance of 156.25. The parameter estimation scheme was actually applied to three such samples of texture to give the parameter



estimates presented in Table 2. For each of the estimates, the search region was chosen empirically so that the maximum occurred in the interior of the region. For the case  $d=1$  all of the  $\lambda$  estimates are greater than unity, and as  $d$  gets larger, the estimated values of  $\lambda$  decrease. The high values of estimated edge density and the fact that these estimates vary greatly for different values of  $d$  is somewhat discomforting. If the assumed rectangular partition process provided an accurate model for the Brodatz textures, values of  $\lambda$  less than unity which remain relatively constant for different values of  $d$  would be expected. That this does not occur can be explained by comparing the properties of the rectangular partition process to the properties of real-world textures. Realizations of the rectangular partition process are composed of regions of constant gray level while most real-world textures are composed of regions of nearly constant gray level. As mentioned in [1], the above properties of the rectangular process results in a large discrete probability mass along the main diagonal of the gray-level co-occurrence matrix while for real-world textures this probability mass will be distributed over the diagonals close to the main diagonal. The high values of estimated edge density which result and the fact that they decrease as  $d$  gets larger are direct result of this mismatch between the model and actual data. Enhancements to the rectangular process model, such as the addition of a white noise field, might eliminate this problem. In the meantime, however, some consolation can be taken from the fact that the estimated parameter values for the three textures are significantly different, which leads to the hope that even though the modeling assumptions are somewhat inaccurate, overall discriminator performance should still be good. This issue will be discussed in the next section.



## V. Discriminator Results:

Making use of the parameter estimates described in the previous section, several discrimination experiments were performed. The 2-D digital filtering implementation approach described in [1] was used as was the Wiener filtering approach to filter design. The specifications and resulting parameters for the designed filters are provided in Table 3. Note the coefficient A described in [1] is not included since it is an overall gain factor, and was taken equal to unity, which will not affect the results. Comparison of the desired and actual frequency responses for the designed filters is provided in Fig.'s 14-16.

The first experiment performed involved processing the same synthetic test image as used in [1]. Recall this test image is composed of three distinct realizations of the rectangular process possessing different parameters, as shown in Fig.'s 17-19.

Since the parameter estimates are quite close to the actual values, and the filters used are the same as those used in [1], it is not surprising that the results, shown in Figs. 17-19, are similar to those in [1]. The case  $d=1$  appears to provide the best results, particularly for the weak and moderate filtering cases. This result tends to disagree with the statement in [1] that a distance equal to the reciprocal of the average edge density of the textures being processed is the optimum distance for texture discrimination. More will be said about this question later.

To test the discriminator on real-world data, the original test image in Fig. 20a was created which contains samples of the three Brodatz texture used in Section III. The upper-left or NW side of the image contains raffia texture data, the right or E side of the image contains grass, and the



bottom or S portion of the image consists of herringbone.

The results of the discriminator using the parameter estimates of Table 2 and the filters specified in Table 3 are presented in Fig.'s 20-22. As was the case for the synthetic test image, a distance of  $d=1$  produced the best results. For this distance, the strong filter provides excellent results comparable to the synthetic test case, while the results for the weak and moderate filters are clearly inferior. This tends to indicate that for the real-world test case, more smoothing is required by the filter to remove incorrectly discriminated areas caused by irregular areas in each texture.

#### VI. Summary and Conclusions

A method for estimating the structural parameters of a specific stochastic texture model has been proposed for use with the texture discrimination scheme described in [1]. This parameter estimation scheme has been shown to provide good results when used on realizations of the rectangular partition process for various choices of model parameters. When applied to selected samples of the Brodatz [4] textures, the parameter estimation scheme gives values which indicate that the rectangular partition process is not an ideal model for real-world textures. However, results of using the texture discriminator on samples containing Brodatz textures are quite good, indicating that the proposed texture discrimination technique can be effective on real-world texture. Several extensions to the procedure are suggested which might improve performance.

For example, results indicate that the rectangular partition process is not an ideal model for real-world textures because it possesses regions



of constant gray level while real world textures usually possess regions of nearly constant gray level. A logical step would be to consider adding a white noise component to the rectangular partition process, and redevelop the expressions for second-order p.d.f.'s which are used in the discriminator and parameter estimator.

Another possible solution to this modeling mismatch might be to include in the pre-processing stage a step which isolates regions of nearly constant gray level and alters the intensity of each pixel within each region to a suitable constant gray level. Hopefully, this step would allow the processed images to retain their textural properties while providing for a closer match between texture and model, resulting in improved discrimination results.

One modification to the texture discrimination system which is proposed is the elimination of the Wiener filtering approach to the 2-D digital filtering implementation. It seems obvious from looking at the frequency responses that the Wiener filters can be replaced by simple lowpass filters parametrized by cutoff frequency. Although this change would not reduce discriminator computational complexity, it would simplify filter design and make it easier to relate discriminator performance to the choice of filter parameters.

One of the questions which must be answered is which value of distance  $d$  between pixels is the best to use in the proposed texture discriminator and parameter estimator. Since the desired objective is to maximize discriminator performance, it seems obvious that the best distance is the value of  $d$  which provides maximum separation of the parameter



estimates for each of the texture classes being considered. The results for the Brodatz test image show this to be true. Despite the fact that the model used provides an inaccurate fit to the textures, the fact that the parameter estimates are significantly different for all three texture classes for the case  $d=1$  results in good discriminator performance.

In any event, it is believed that the proposed texture discriminator can be used to provide effective performance in a variety of real-world texture discrimination problems. Further work is being done to improve discriminator performance and establish the efficacy of this approach as applied to other real world texture problems.

#### References

1. J. W. McQuestino, R. W. Fries, and A. L. Vickers, "Texture Discrimination Based Upon An Assumed Stochastic Texture Model", submitted to IEEE Trans. on Pattern Analysis and Machine Intelligence.
2. P. M. Haralick, K. Shanmugam and I. Dinstein, "Textural Features for Image Classification", IEEE Trans. Syst., Man, and Cybern., vol. SMC-3, pp. 610-621, Nov. 1973.
3. W. K. Pratt, Digital Image Processing, Wiley - Interscience, New York, 1978, Chap. 12.
4. P. Brodatz, Textures: A Photographic Album for Artists and Designers. Dover, New York, 1956.



Texture Parameters	$\hat{\rho}_{ML}$	$\hat{\lambda}_{ML}$	$d=1$		$d=2$		$d=3$	
	$\hat{\rho}_{ML}$	$\hat{\lambda}_{ML}$	$\hat{\rho}_{ML}$	$\hat{\lambda}_{ML}$	$\hat{\rho}_{ML}$	$\hat{\lambda}_{ML}$	$\hat{\rho}_{ML}$	$\hat{\lambda}_{ML}$
$\rho = 0.0,$ $\lambda = 0.167$	0.00	0.16	0.00	0.16	0.00	0.16	0.00	0.157
$\rho = 0.5,$ $\lambda = 0.33$	0.50	0.31	0.50	0.32	0.50	0.32	0.50	0.325
$\rho = 0.0,$ $\lambda = 0.33$	0.00	0.30	0.00	0.32	0.00	0.32	0.00	0.325

Table 1

Parameter Estimates for Realizations  
of Rectangular Partition Process

Texture Class	$\hat{\rho}_{ML}$	$\hat{\lambda}_{ML}$	$d=1$		$d=2$		$d=3$	
	$\hat{\rho}_{ML}$	$\hat{\lambda}_{ML}$	$\hat{\rho}_{ML}$	$\hat{\lambda}_{ML}$	$\hat{\rho}_{ML}$	$\hat{\lambda}_{ML}$	$\hat{\rho}_{ML}$	$\hat{\lambda}_{ML}$
Grass	.90	2.05	.70	1.15	.575	.85	.575	.85
Raffia	.95	2.50	.875	1.35	.825	1.00	.825	1.00
Herringbone	.95	3.25	.825	1.50	.615	1.05	.615	1.05

Table 2

Parameter Estimates for Sequences of Products



Filter #	Interference Characteristic	$\lambda_i$	$\rho_i$	$\gamma_i, \text{dB}$	$\lambda_t$	$f_t$	$\gamma_t, \text{dB}$	$a_{10}$	$a_{11}$	$b_{10}$	$b_{11}$
1	Weak d=1	2.05	0.0	-6	0.0125	0.0	0	-.9581	.9277	-.2986	.2118
2	Moderate d=1	2.05	0.0	0	0.0125	0.0	0	-.9590	.9263	-.4062	.3508
3	Strong d=1	2.05	0.5	6	0.0125	0.0	0	-.9606	.9226	-.7944	.6933
4	Weak d=2	1.15	0.0	-6	0.0125	0.0	0	-.9587	.9266	-.3810	.3330
5	Moderate d=2	1.15	0.0	0	0.0125	0.0	0	-.9592	.9249	-.5038	.4360
6	Strong d=2	1.15	0.5	6	0.0125	0.0	0	-.9604	.9222	-.8492	.7987
7	Weak d=3	.85	0.0	-6	0.0125	0.0	0	-.9589	.9262	-.4320	.4082
8	Moderate d=3	.85	0.0	0	0.0125	0.0	0	-.9588	.9243	-.5853	.6158
9	Strong d=3	.85	0.5	0	0.0125	0.0	0	-.9604	.9221	-.8565	.8136

Table 3

Filter Parameters for Brodatz Experiment

$$\gamma_n = -10 \text{ dB}$$



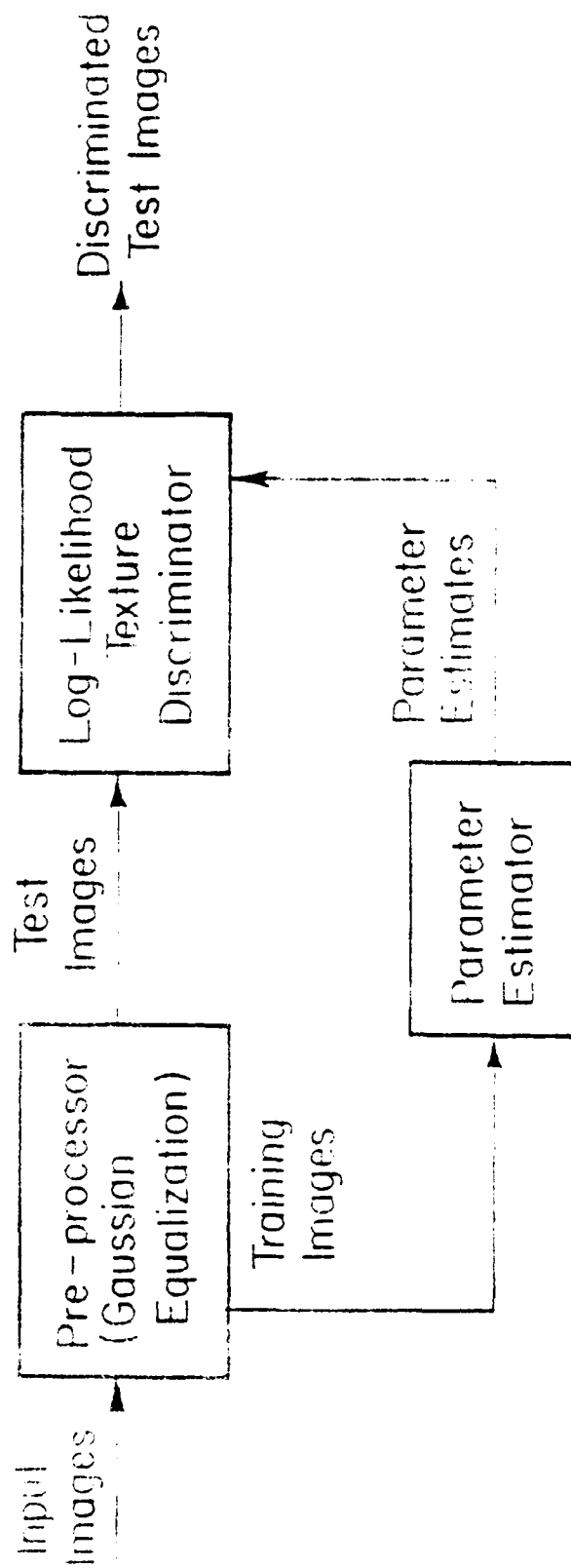
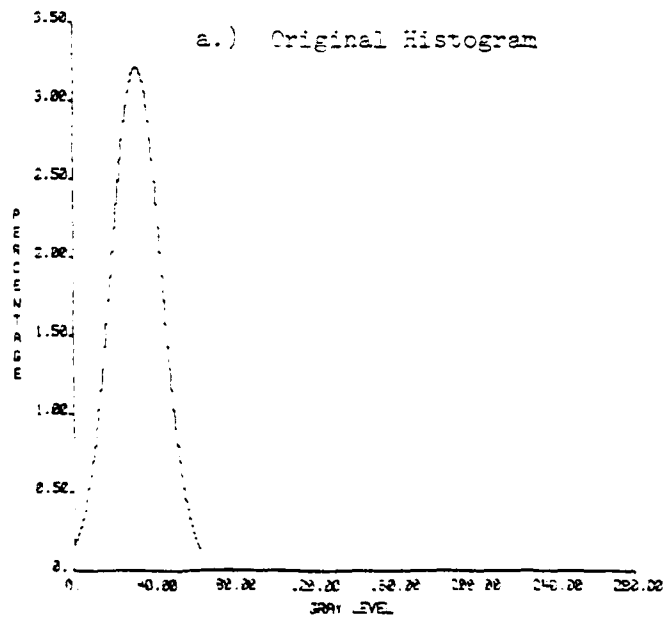
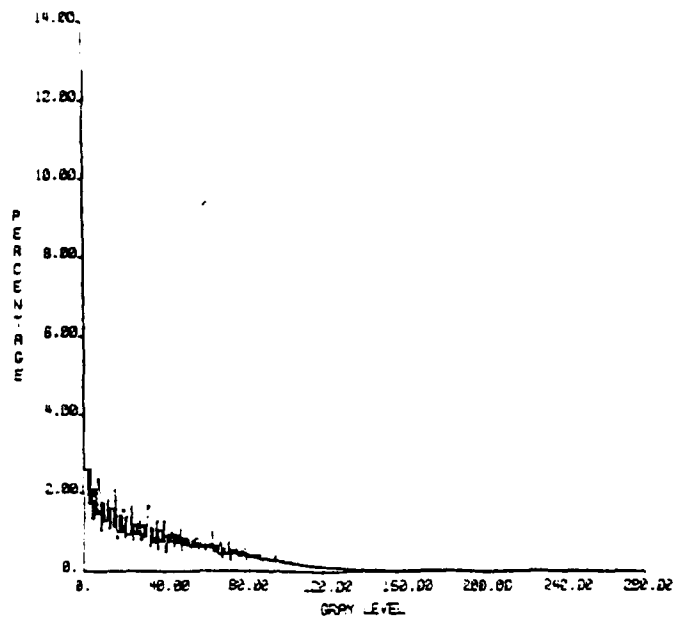


Figure 1

Block Diagram of Texture Discrimination System Utilizing

Parameter Estimates Derived from a Training Set

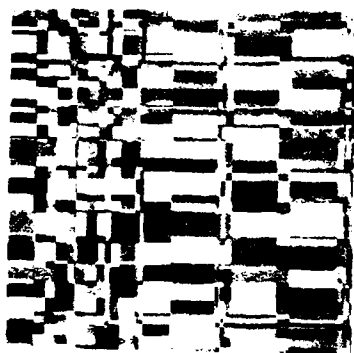




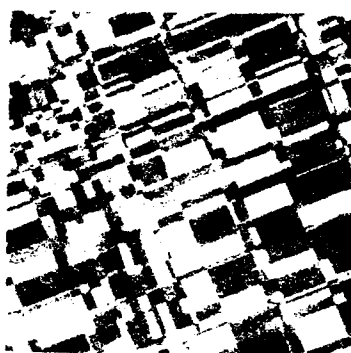
b.) Histogram After Equalization

Figure 2  
Effect of Gaussian Equalization  
on Image Histogram

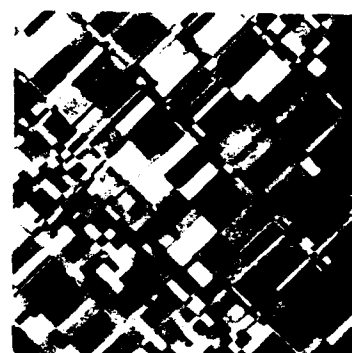




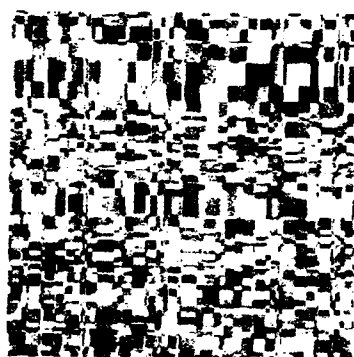
1.)  $\lambda=0.367, v=0.0$   
 $\theta=0$



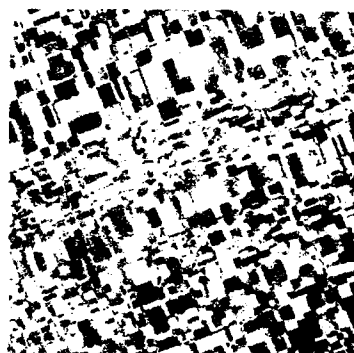
1.)  $\lambda=0.367, v=0.0$   
 $\theta=45^\circ$



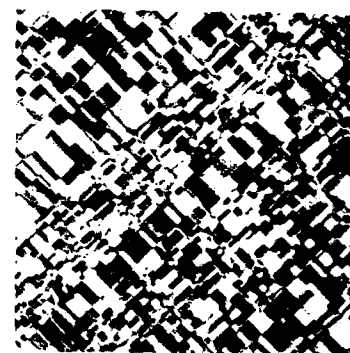
1.)  $\lambda=0.367, v=0.0$   
 $\theta=90^\circ$



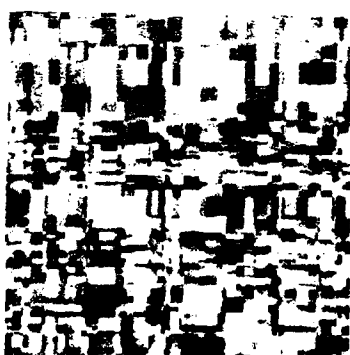
2.)  $\lambda=0.33, v=0.0$   
 $\theta=0$



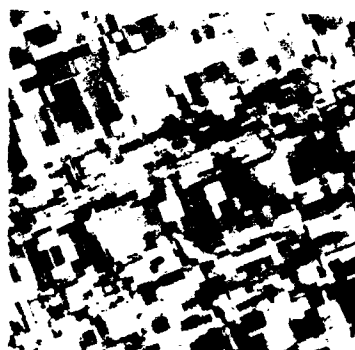
2.)  $\lambda=0.33, v=0.0$   
 $\theta=45^\circ$



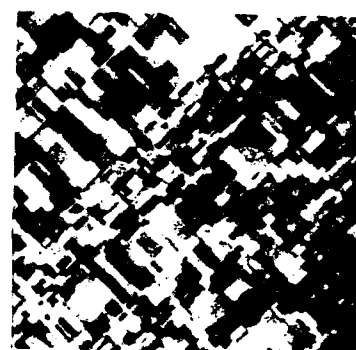
2.)  $\lambda=0.33, v=0.0$   
 $\theta=90^\circ$



3.)  $\lambda=0.33, v=0.5$   
 $\theta=0$



3.)  $\lambda=0.33, v=0.5$   
 $\theta=45^\circ$



3.)  $\lambda=0.33, v=0.5$   
 $\theta=90^\circ$

Figure 1

Collected Realizations of a Stochastic Process



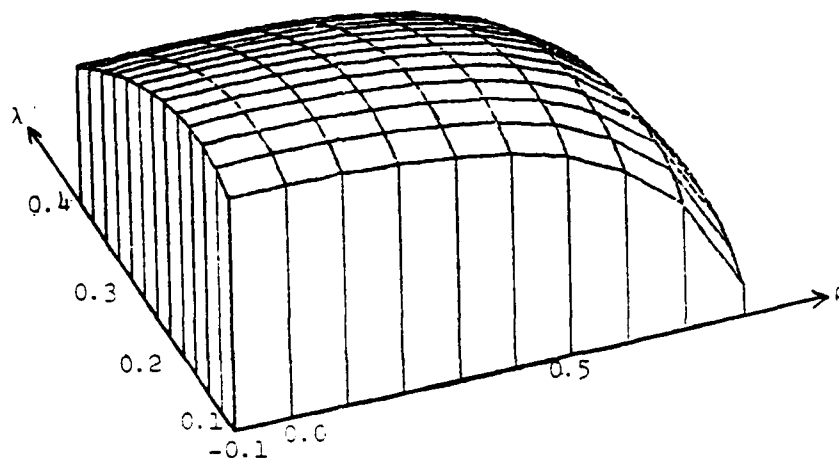


Figure 4

Log-Likelihood Surface for Rectangular Partition Process;

$\lambda=0.167$ ,  $\rho=0.0$ ,  $d=1$ .

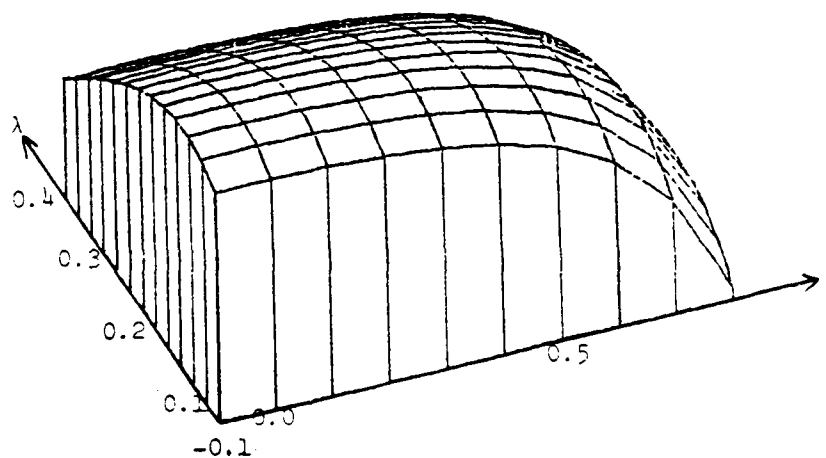


Figure 5

Log-Likelihood Surface for Rectangular Partition Process;

$\lambda=0.167$ ,  $\rho=0.0$ ,  $d=2$ .



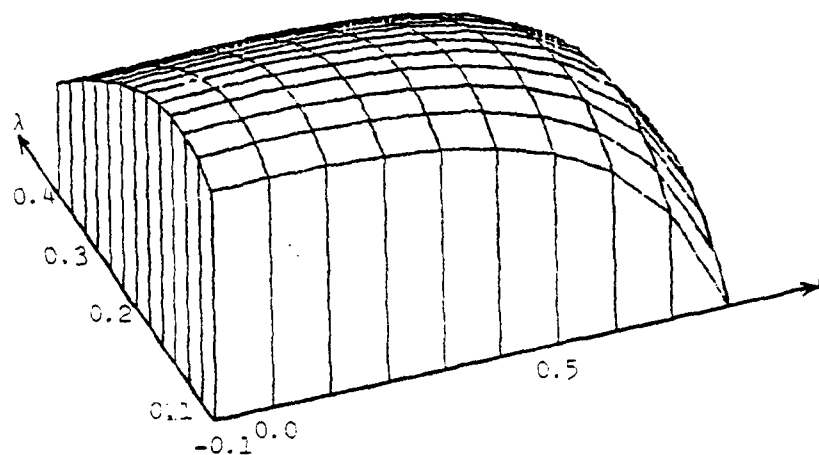


Figure 6

Log-Likelihood Surface for Rectangular Partition Process;

$$\lambda=0.167, \rho=0.0, d=3.$$

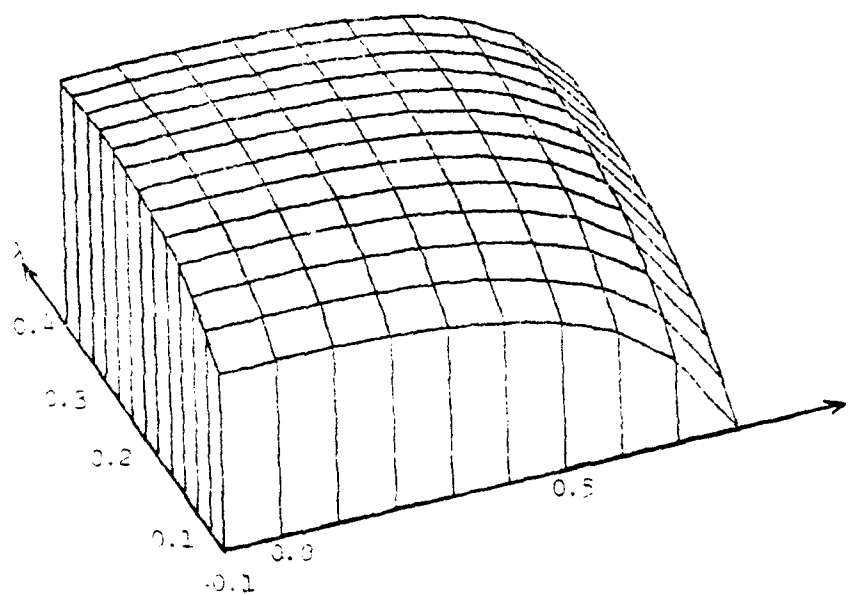


Figure 7

Log-Likelihood Surface for Rectangular Partition Process;

$$\lambda=0.33, \rho=0.0, d=1.$$



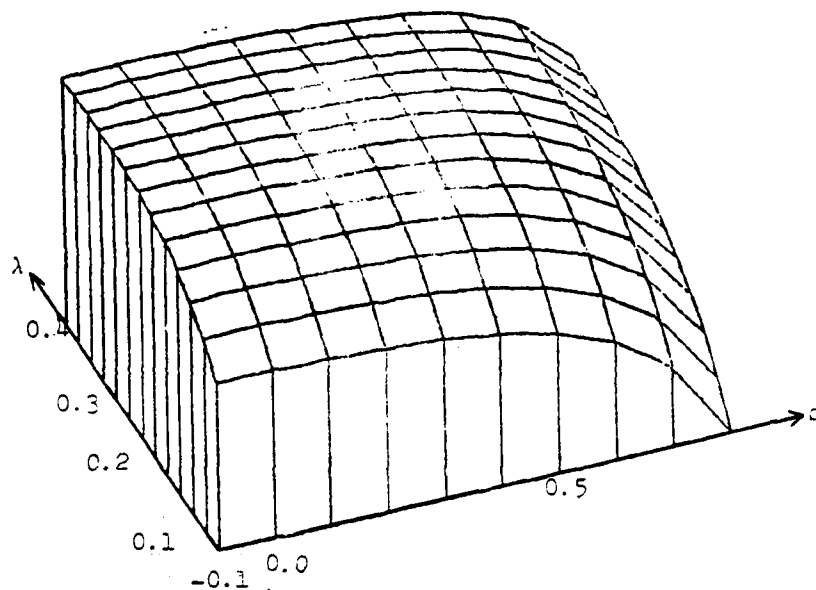


Figure 8

Log-Likelihood Surface for Rectangular Partition Process;  
 $\lambda=0.33$ ,  $\mu=0.0$ ,  $d=2$

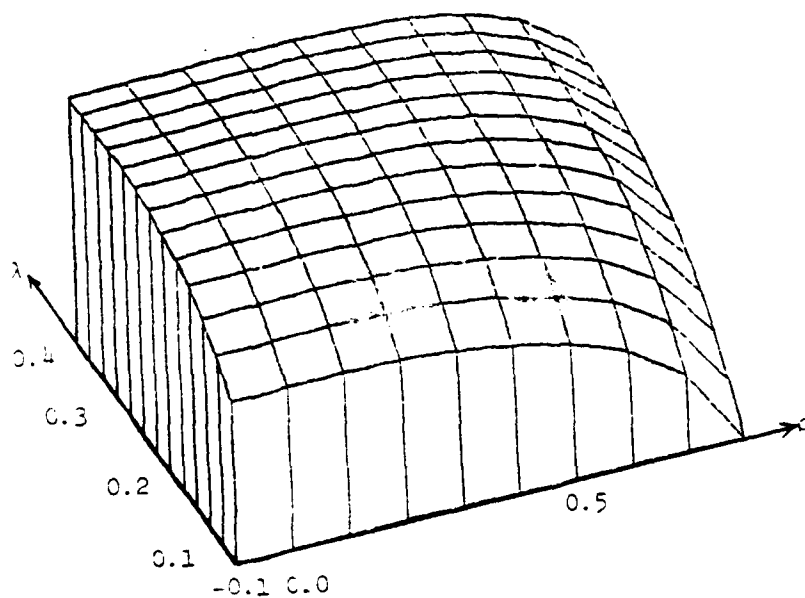


Figure 9

Log-Likelihood Surface for Rectangular Partition Process;  
 $\lambda=0.33$ ,  $\mu=0.0$ ,  $d=1$



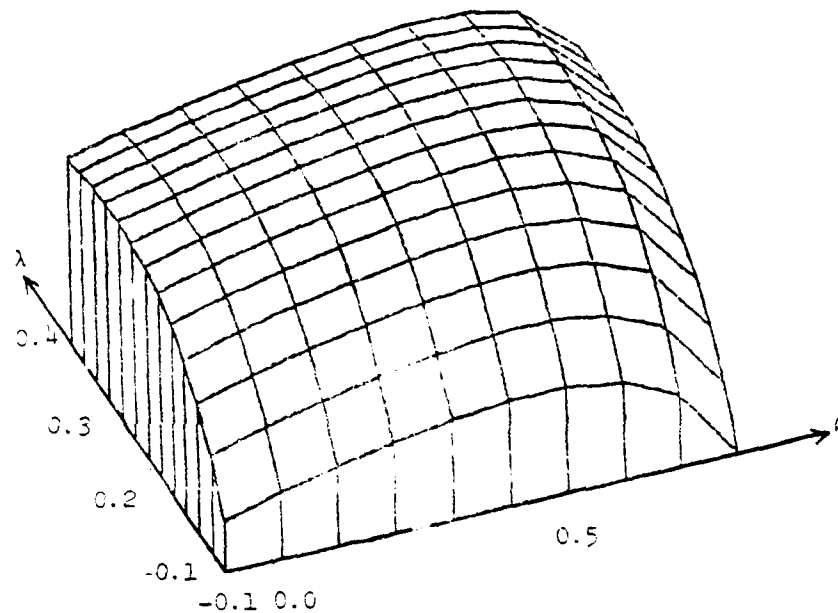


Figure 10

Log-Likelihood Surface for Rectangular Partition Process;

$\lambda=0.33$ ,  $\rho=0.5$ ,  $d=1$ .

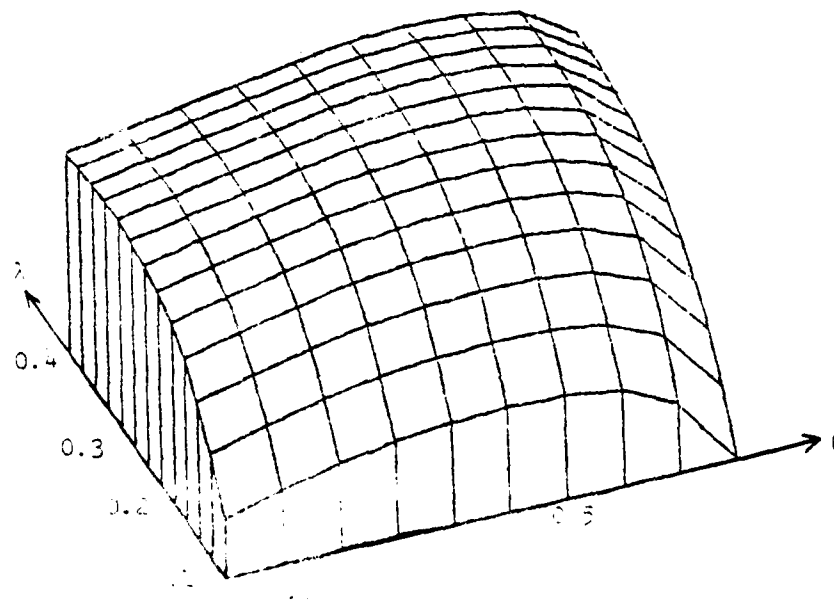


Figure 11

Log-Likelihood Surface for Rectangular Partition Process;

$\lambda=0.33$ ,  $\rho=0.5$ ,  $d=1$ .



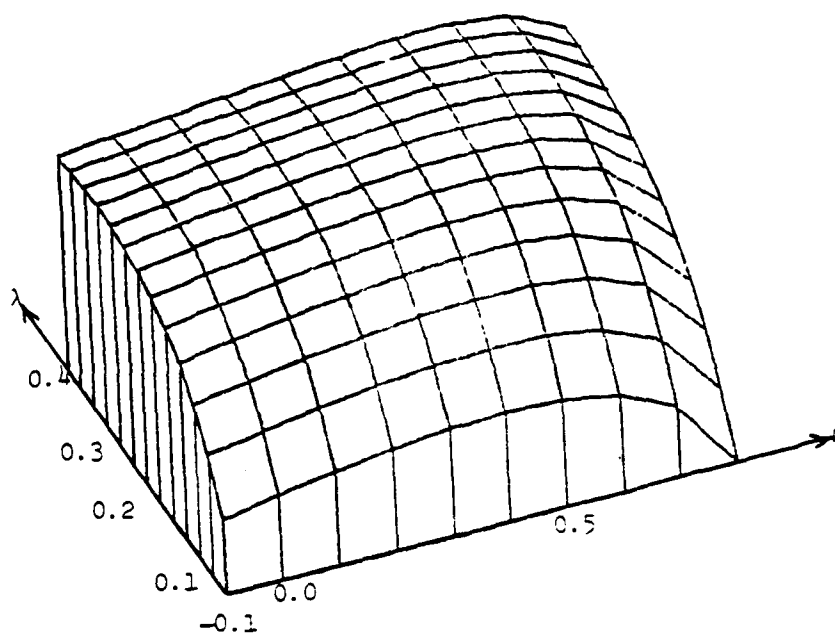
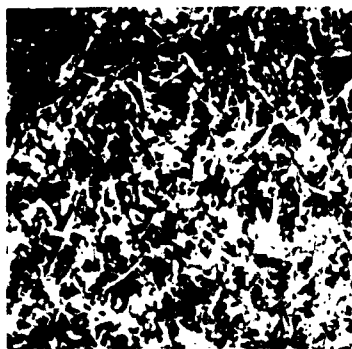
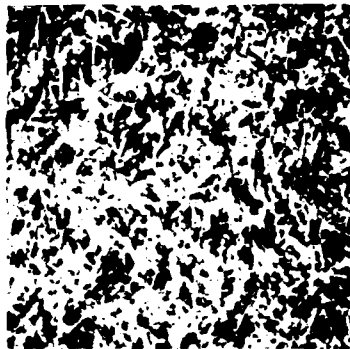


Figure 12  
Log-Likelihood Surface for Rectangular Partition Process;  
 $\lambda=0.33$ ,  $\rho=0.5$ ,  $d=3$ .

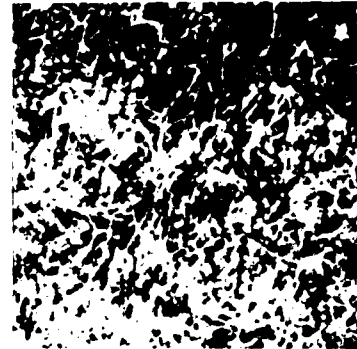




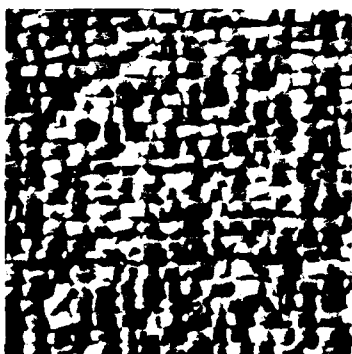
a.) Grass Sample 1



b.) Grass Sample 2



c.) Grass Sample 3



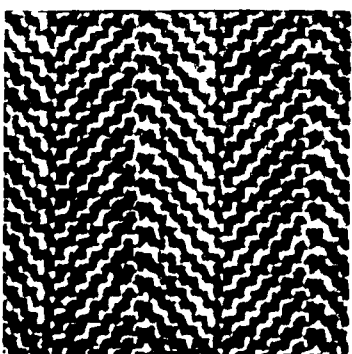
d.) Raffia Sample 1



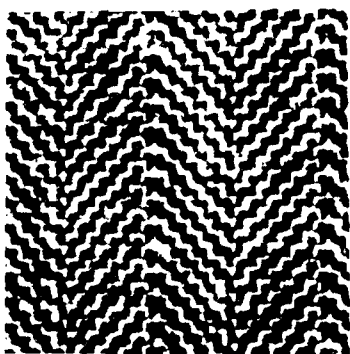
e.) Raffia Sample 2



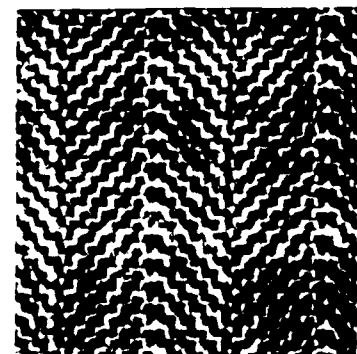
f.) Raffia Sample 3



g.) Herringbone  
Sample 1



h.) Herringbone  
Sample 2

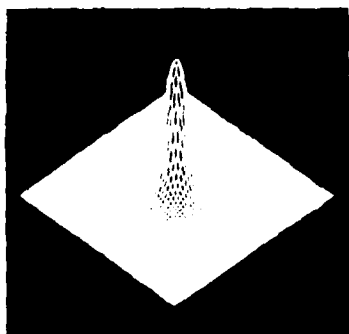


i.) Herringbone  
Sample 3

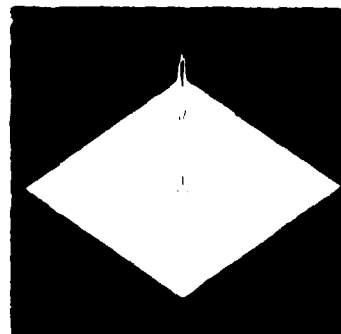
Figure 13

Selected Samples of Brodatz Textures

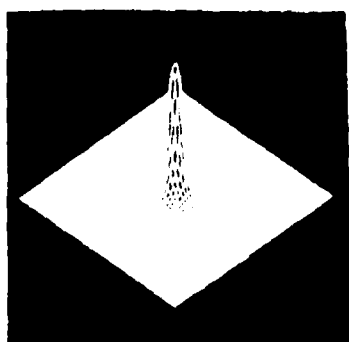




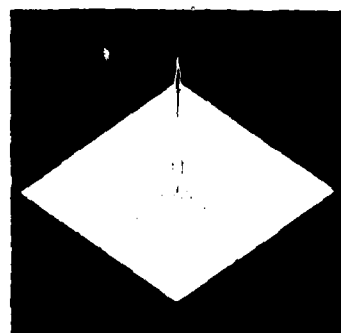
a.) Desired Response  
for Filter 1



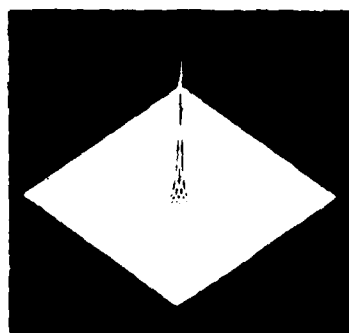
b.) Actual Response  
for Filter 1



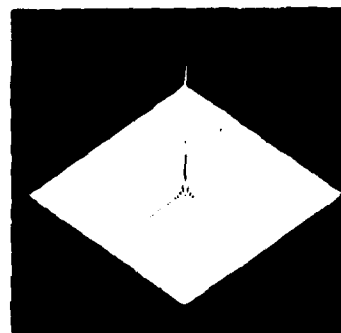
c.) Desired Response  
for Filter 2



d.) Actual Response  
for Filter 2



e.) Desired Response  
for Filter 3

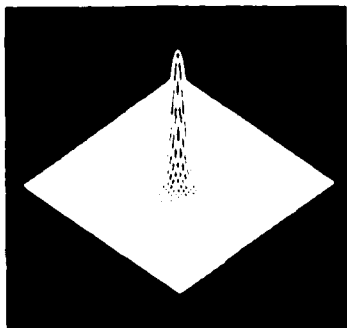


f.) Actual Response  
for Filter 3

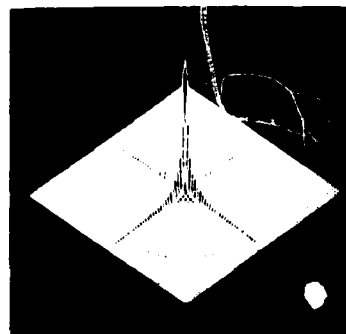
Figure 14

Frequency Responses of Desired and Actual Filters for  $\alpha=1$

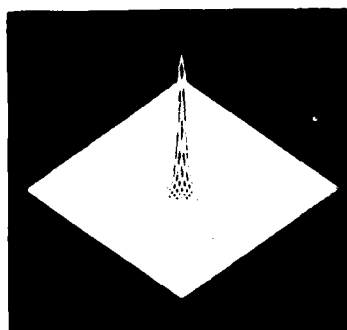




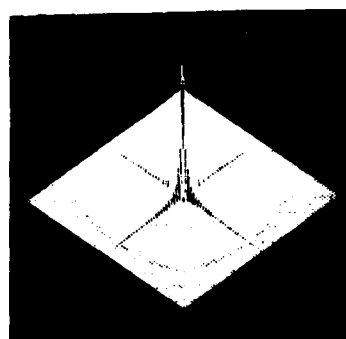
a.) Desired Response  
for Filter 4



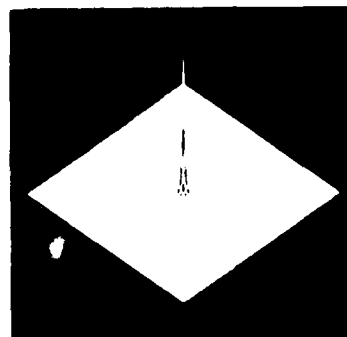
b.) Actual Response  
for Filter 4



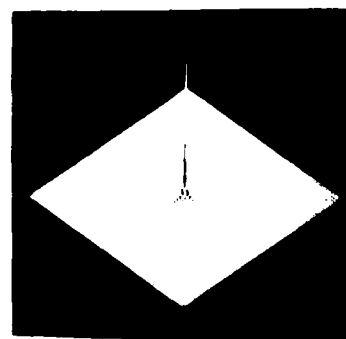
c.) Desired Response  
for Filter 5



d.) Actual Response  
for Filter 5



e.) Desired Response  
for Filter 6

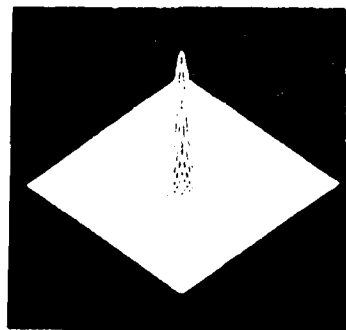


f.) Actual Response  
for Filter 6

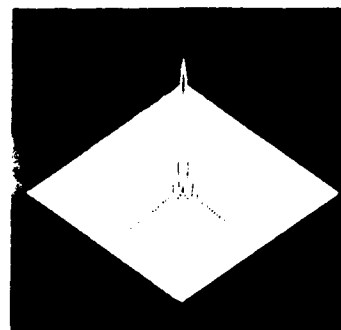
Figure 15

Frequency Responses of Desired and Actual Filters for  $d=2$

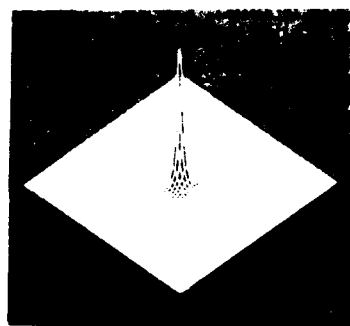




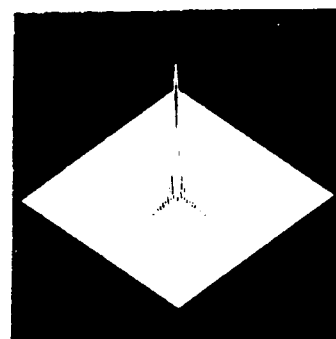
a.) Desired Response  
for Filter 7



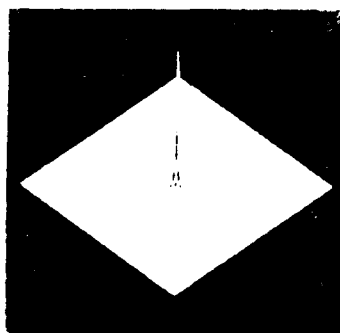
b.) Actual Response  
for Filter 7



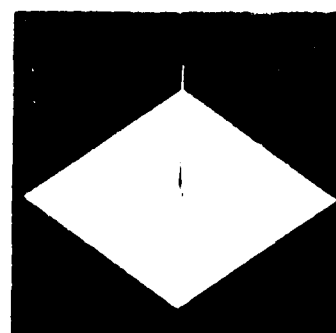
c.) Desired Response  
for Filter 8



d.) Actual Response  
for Filter 8



e.) Desired Response  
for Filter 9

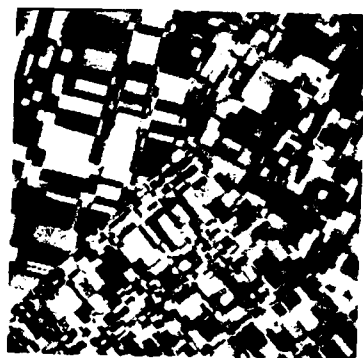


f.) Actual Response  
for Filter 9

Figure 1

Frequency Responses of Desired and Actual Filter Responses





a.) Original; NW,  $\rho=0.0$ ,  
 $\lambda=0.16$ ; NE,  $\rho=0.5$ ,  
 $\lambda=0.33$ ; S,  $\rho=0.0$ ,  
 $\lambda=0.33$



b.) Weak Interference



c.) Moderate Interference

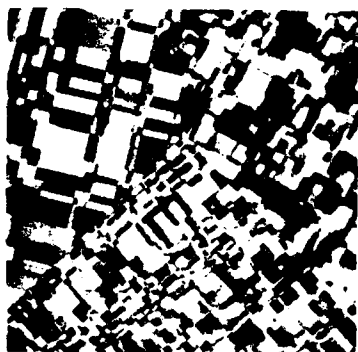


d.) Strong Interference

Figure 17

Performance of Log-Likelihood Discriminator  
 Using Parameter Estimates with  $d=1$





a.) Original: NW,  $p=0.0$   
 $\lambda=0.16$ ; NE,  $p=0.5$ ,  
 $\lambda=0.33$ ; S,  $p=0.0$ ,  
 $\lambda=0.33$



b.) Weak Interference



c.) Moderate Interference

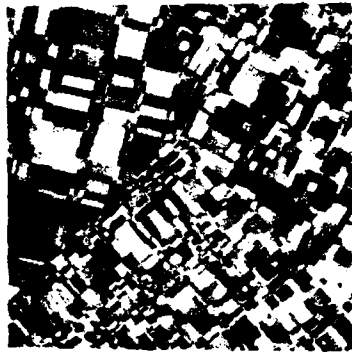


d.) Strong Interference

Figure 18

Performance of Log-Likelihood Discriminator  
 Using Parameter Estimates with  $d=0$





a.) Original; NW,  $\rho=0.0$   
 $\lambda=0.16$ ; NE,  $\rho=0.5$ ,  
 $\lambda=0.33$ ; S,  $\rho=0.0$ ,  
 $\lambda=0.33$



b.) Weak Interference



c.) Moderate Interference

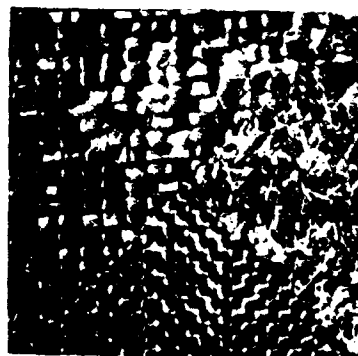


d.) Strong Interference

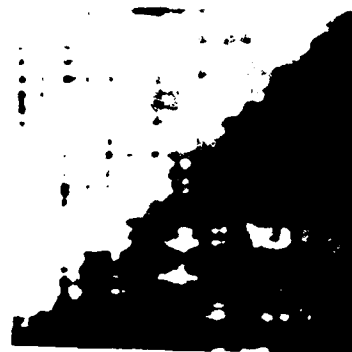
Figure 19

Performance of Log-Likelihood Discriminator  
 Using Parameter Estimates with  $d=3$





a.) Original; NW, Raffia;  
E, Grass; S, Herring-  
bone



b.) Filter 1  
Weak Interference



c.) Filter 2  
Moderate Interference

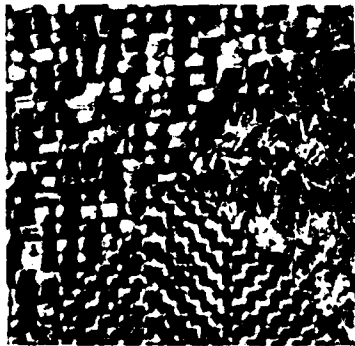


d.) Filter 3  
Strong Interference

Figure 14

Performance of Log-Likelihood Discriminator  
Using Parameter Estimates with  $d=1$





a.) Original; NW, Raffia;  
E, Grass; S, Herring-  
bone



b.) Filter 4  
Weak Interference



c.) Filter 5  
Moderate Interference

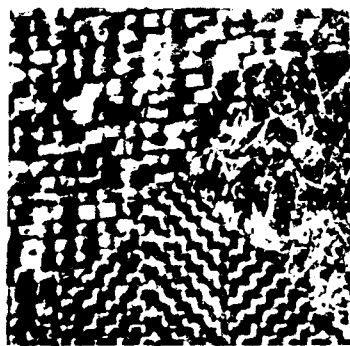


d.) Filter 6  
Strong Interference

Figure 21

Performance of Log-Likelihood Discriminator  
Using Parameter Estimates with  $d=2$





a.) Original; LW, Laffla;  
E, Gross; R. Weirring-  
bone



b.) Filter 7  
Weak Interference



c.) Filter 8  
Moderate Interference



d.) Filter 9  
Strong Interference

Figure 22

Performance of Log-Likelihood Discriminator  
Using Parameter Estimates with  $d=3$





## *MISSION of Rome Air Development Center*

RADC plans and executes research, development, test and selected acquisition programs in support of Command, Control Communications and Intelligence (C<sup>3</sup>I) activities. Technical and engineering support within areas of technical competence is provided to ESD Program Offices (POs) and other ESD elements. The principal technical mission areas are communications, electromagnetic guidance and control, surveillance of ground and aerospace objects, intelligence data collection and handling, information system technology, ionospheric propagation, solid state sciences, microwave physics and electronic reliability, maintainability and compatibility.



